Detection of Faults and Barriers on Automated Large-Scale 2-D EWOD Digital Microfluidics

Chunqiao Li, Wei Wang, Lei Chao, Xiumin Ji, and Jia Zhou

***Abstract*— In lab on chip applications, on-chip detection of faults and barriers on electrowetting-on-dielectric (EWOD) digital microfluidics (DMFs) shows great significance for precise results. In this paper, we develop a sensor-free all-electronic integrated system based on one set of impedance detection circuits for all electrodes. Calibration, precise, and real-time droplet detection and result exhibition are realized through the operating electronic hardware and software. A specific voltage transforming method is proposed for fast detection. A significant practice of cyberphysical coupling in digital microfluidics is demonstrated through a 10 × 10 DMF. The detection sensitivity and consistency of the system shows the feasibility of the system. The 100% agreement between the experimental results and the real map of droplets on DMF demonstrates the capability of the system applicable for large-scale 2-D EWOD DMFs, and provides preliminary requirements for auto-routing. [2017-0164]**

***Index Terms*— Electro-wetting, fault and barrier detection, impedance detection, large-scale digital microfluidics (DMF).**

I. Introduction

RAPID operations and accurate results are all microfluidic biochip's design aim. However, in practical electrowetting-on-dielectric (EWOD) digital microfluidics, no matter conventional DMFs or recently proposed microelectrode dot array (MEDA) [1], on-chip faults and barriers always hinder the ongoing experiment or destroy the result [2], [3].

Dielectric breakdown is a main fault that will result in droplets unmovable. Discovering the breakdown sites in time is important. On-chip barriers can be classified into two types, absolute ones and relative ones. The absolute ones are the residues of reagents or biomolecules. This sort of barrier not only affects the quantitative analysis of reagent dosing [4], but blocks the actuated droplets. As to the relative barriers, all droplets except the one that is being actuated can be seen as "barriers" [5]. Whichever barrier it is, the occupied sites should be avoided for droplet routing. It is a must to detect the distribution of these barriers.

However, to our best knowledge, in conventional DMFs, except that Hu *et al.* [6], [7] presented experimental demonstrations of fault recovery and Gao *et al.* [5] achieved fault tolerance by using a fuzzy-enhanced control system, almost other research groups are staying at modeling and simulation [8]–[10]. They utilized synthesis tools to generate optimized schedule of fluidic operations or compute droplet transportation routes, *etc*. A main reason for conventional DMFs' decelerated development is that there lacks proper sensors for real-time detection [3]. K. Hu's system needed a set of sensing hardware at every individual checkpoint, which limits its application in large scale, while J. Gao's had to switch the circuit states between droplets actuation and signal acquisition, which increases the system complexity and timing overhead.

To break through this dilemma, utilizing IC technology to integrate processing circuits seems to be the only choice. Therefore, Lai *et al.* [11] and Li *et al.* [12], [13] integrated an activation circuit and a sensing circuit beneath every microelectrode on MEDA chips. And Hadwen *et al.* [14] and Kalsi *et al.* [15] did the similar work on the thin film transistors (TFT) based EWOD chips. As expected, the integrated capacitive sensors worked very well. However, although there have even been some synthesis solutions of MEDA [3], [12], [13], [16], this novel customized architecture needed to be built up on an IC chip. The fabrication must be much more complex compared with conventional EWOD systems, and the cost may be high. It still has a distance to mass applications nowadays.

Recently [17], [18], presented a simple impedance measurement method to achieve precise liquid sensing, which only needs several extra passive devices such as resistors and capacitors. Moreover, this idea incorporated the sensing circuit into the actuation circuit of EWOD. Only one set of sensing hardware was required for the whole EWOD chip. Resembling serial data reading, the EWOD chip's sites will be sensed in sequence. This impedance technique can be a promising candidate for fault and barrier detection on a portable large-scale 2D EWOD DMF.

Nevertheless, an obvious weakness in [17] and [18] is that their sensing hardware and software relied severely on a set of products of NI (National Instruments) which is expensive

Manuscript received July 27, 2017; revised September 25, 2017; accepted October 14, 2017. Date of publication October 30, 2017; date of current version November 29, 2017. This work was supported by the National Science Foundation of China under Grant 61674043. Subject Editor Y. Zohar. *(Corresponding author: Chunqiao Li.)*

C. Li, W. Wang, and J. Zhou are with the ASIC and System State Key Laboratory, School of Microelectronics, Fudan University, Shanghai 200433, China (e-mail: 15210720067@fudan.edu.cn; 14110720019@fudan.edu.cn; jia.zhou@fudan.edu.cn).

L. Chao was with the ASIC and System State Key Laboratory, School of Microelectronics, Fudan University, Shanghai 200433, China. She is now with NXP Semiconductors, Tianjin 120000, China (e-mail: 14210720056@fudan.edu.cn).

X. Ji was with the ASIC and System State Key Laboratory, School of Microelectronics, Fudan University, Shanghai 200433, China. She is now with AMD, Shanghai 201203, China (e-mail: 14210720068@fudan.edu.cn).

Color versions of one or more of the figures in this paper are available online at http://ieeexplore.ieee.org.

Digital Object Identifier 10.1109/JMEMS.2017.2764139

TABLE I
COMPARISON OF MEDA, TFT, CONVENTIONAL DMFB, AND OUR SYSTEM

Platform	Electrode size	Integrating actuators	Detection technique	Limit of detection	Scalability	Portability	Detection manner	Cost
MEDA[1,3,12,13]	~100μm	Yes	Integrating capacitance sensors	Possibly the same as TFT's	Very high	Possibly high	Parallel	High
TFT[14,15]	~210μm	Yes	Integrating capacitance sensors	~5nL	Very high	Very high	Parallel	High
conventional DMFB[2,5-7]	~1mm	No	Capacitance sensing+Ring oscillator circuit	~2nL	Low	Low	Parallel	Up to control pins and detection site number
Our system	1.74mm	No	Impedance sensing	~3.2nL[1]	High	High	Serial[2]	Low

[1] This data was estimated by the electrode size, gap distance between the two plates, and the detection sensitivity. In our system, the electrode size was 1.74mm×1.74mm and the gap distance was about 150μm.
[2] Serial detection time is up to the electrode number since every electrode will usually consume about 10ms.

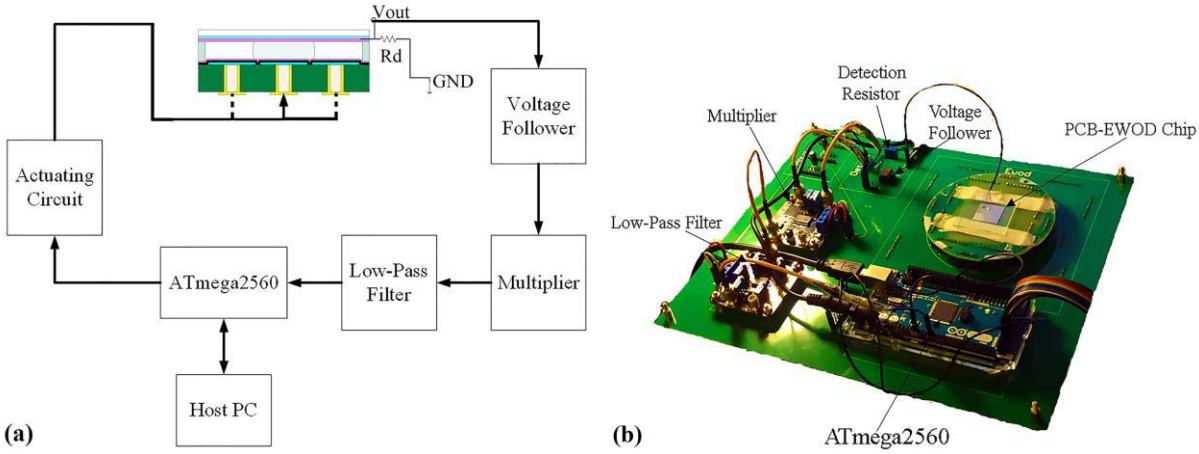

Fig. 1. Home-made low-cost system aiming for large-scale 2D DMF. The custom pogo-pin connectors enable plug-pull between the PCB-EWOD chip and the substrate board. (a) Signal flow; (b) Prototype picture.

and non-portable. In addition, the calibration method in [17] relayed on evaporation of solvents at room temperature, which is so slow that it is inadequate to calibrate a large-scale 2D EWOD DMF. Fobel *et al.* [19] may have noticed the portability problem of [17] and [18]. They used a webcam and other hardware/software building an open source platform named DropBot, which can real-time monitor droplet position, velocity, *etc.* on a 15 × 4 array.

In this paper, inspired by the impedance method, we show an all-electronic integrated system for breakdown sites and on-chip barriers detection, which is in low-cost and portable. Table I lists electrode size, integrating actuators, detection technique, limit of detection, scalability, portability, detection manner, and cost for MEDA, TFT, conventional DMFB, and our system. The comparison shows that our system is a good candidate for EWOD applications, providing respectable simplicity and precision at low costs. We fabricate the 10 × 10 EWOD device on top of a double-layer printed circuit board (PCB). A novel calibration mean which is specially designed for large-scale 2D EWOD DMFs will be presented. The rest of paper is organized as follows. Section II describes the theory and method of real-time impedance detection and measurement to liquid fraction, *i.e.* the novel calibration mean. Experimental details, *e.g.* system calibration, faults and barriers detection and exhibition are discussed in Section III. Section IV concludes the paper.

II. THEORY AND METHOD

EWOD takes advantage of electrohydrodynamic forces, and they can provide high droplet speeds with relatively simple geometries. For droplet motion, a certain contact angle difference is required by applying adequate drive voltage [1].

Our home-made low-cost system is shown in Fig. 1. It is installed on a double-side PCB of 27 cm × 23 cm × 1.6 mm. The pogo-pin connectors enable plug-pull between the PCB-EWOD chip and the substrate board. Fig. 1(a) shows the signal flow of the system. Fig. 1(b) is the prototype photo of the whole system. The whole system houses eight modules. Besides the PCB-EWOD chip itself, a slide detection

resistor R_d, a voltage follower (LM110J-8, National Semiconductor), a multiplier (AD630, Analog Devices), a low-pass filter (UAF42, Texas Instruments), a microcontroller (Arduino Mega2560, SmartProjects, Italy), an actuating circuit and a host PC are included. The actuating circuit comprises of AND gates (74HC08D, quad 2-input AND gate, Philips Semiconductors), solid state relays (SSR, AQH2223, Panasonic Corporation), *etc.*, which can manipulate 100 individual electrodes using 10 row signals and 10 column signals. It should be noted that due to the leakage currents of SSRs, even when no electrode is activated, detecting signal still exists. We use dotted lines to depict these leakage currents.

Based on the actuating circuit and real time impedance detection, our system has the capability of droplet driving, sensing and visualizing. Through proper combination, these diverse functionalities form up a feed-back control loop.

Droplet driving relies on the actuating circuit. When the actuating voltage V_{AC} is higher than V_{th}(V_{th} is the threshold voltage for moving a droplet) and applied to the EWOD chip, the corresponding droplet will be moved according to the microcontroller instructions.

Droplet sensing is inspired by the impedance method [17]. Assuming $V_{AC} = Asin(\omega t)$, the output detection signal is $V_{out} = \alpha Asin(\omega t + \theta)$, where $0 < \alpha < 1$. To match circuit impedance, the voltage follower is needed. The tracked signal V_{out} will be delivered to the multiplier to multiply itself, whose product is shown in eqn (1).

$$V_{out}^2 = \alpha^2 A^2 sin^2(\omega t + \theta) = \frac{1}{2}\alpha^2 A^2 - \frac{1}{2}\alpha^2 A^2 \cos(2\omega t + 2\theta) \tag{1}$$

Then, through the low-pass filter, a DC voltage signal $\frac{1}{2}\alpha^2 A^2$ corresponding to the EWOD device's impedance is extracted. Finally, using an analog to digital converter (ADC, 10 bits resolution) of the microcontroller, the DC signal is acquired.

Droplet visualizing is realized by exhibiting the real time detection result. A JAVA software was specially composed.

Two major detection methods used in this paper is being explained in the following sections. One is the impedance method theory. The other is the novel measurement mean of liquid fraction.

A. Real-Time Impedance Detection

Fig. 2 gives the diagram and electrical model of circuit for droplet driving, and faults and barriers detection on EWOD device. Fig. 2(a) is a simplified figure of driving and detecting circuit of EWOD chip. It is clear that the detection circuit that only owns a resistor R_d is incorporated into the actuation circuit. In the electrical model of EWOD shown in Fig. 2(b), the dielectric layer and the droplet can be treated as parallel resistors and capacitors connected in series. When a discrete droplet aligns with the buried electrode, a capacitor C_{di} and a resistor R_{di} are formed between the bottom surface of the droplet and the buried electrode. C_{di} is a function of the droplet volume, which only depends upon the area that the droplet covers. R_w and C_w represent the electrical property of the liquid. $R_{di}^{1,2\cdots}$ (GΩ) and $C_{di}^{1,2\cdots}$ (fF) respectively denote the equivalent resistors and capacitors of other dry sites.

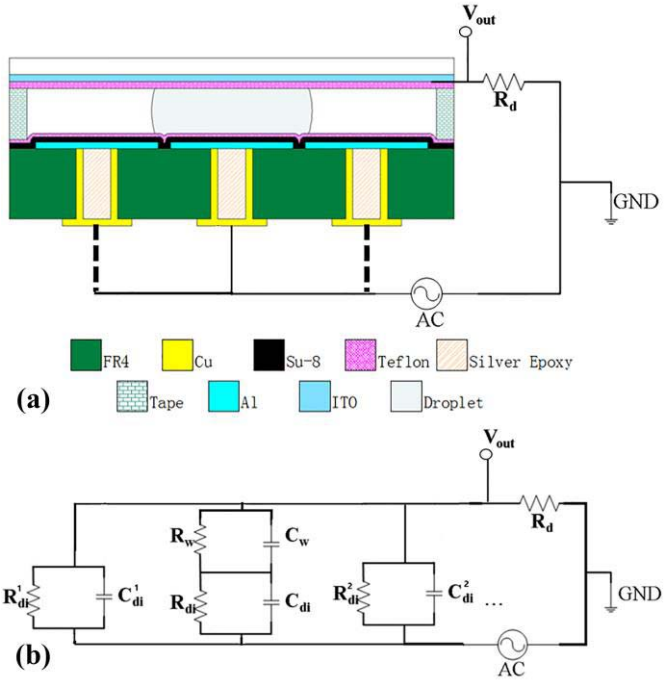

Fig. 2. Diagram of fault and barrier detection on EWOD device. (a) Simplified figure of driving and detecting circuit of EWOD device; (b) Driving and detecting circuit with model of impedance for EWOD. The dielectric layer and the droplet can be treated as parallel resistors and capacitors connected in series.

Generally, $R_{di}^{1,2\cdots}$ and $C_{di}^{1,2\cdots}$ are negligible [20], [21]. According to $\frac{R_w}{1+j\omega R_w C_w} \ll \frac{R_{di}}{1+j\omega R_{di} C_{di}}$, the relationship between V_{out} and C_{di} and R_{di} can be deduced as shown in eqn (2).

$$V_{out} = \frac{R_d V_{AC}}{\frac{R_{di}}{1+j\omega R_{di} C_{di}} + R_d} \tag{2}$$

Accordingly, the potential V_{out} will change once a droplet is laid on a buried electrode, *i.e.* C_{di} increases, or a site is broken down, *i.e.* R_{di} decreases. This principle is the core of the real-time impedance detection method. Through analyzing the diverse V_{out}, the faults and barriers can be recognized.

B. Quick Measurement of Liquid Fraction

Sensitivity and consistency of droplet on-chip detection are two key calibration aspects of a large-scale 2D EWOD DMF.

The calibration method comprises two main steps. The first step is to measure the faults and barriers in a low actuation voltage, *i.e.* $V_{AC} < V_{th}$. The second is to transform the measured data, which makes the data used in a normal circumstance, *i.e.* $V_{AC} > V_{th}$. V_L and V_H are employed to represent V_{AC} under the circumstances of $V_{AC} < V_{th}$ and $V_{AC} > V_{th}$, respectively.

The measurement procedure is shown as following. A deionized water droplet is put on an electrode region (3 rows $\times$ 3 columns) of the 2D EWOD DMF as shown in Fig. 3(a). The liquid keeps a normal circle shape in top view. Dotted lines enclosed area represents a partial region where the liquid covers on the buried electrodes. x_{liq} is used to denote

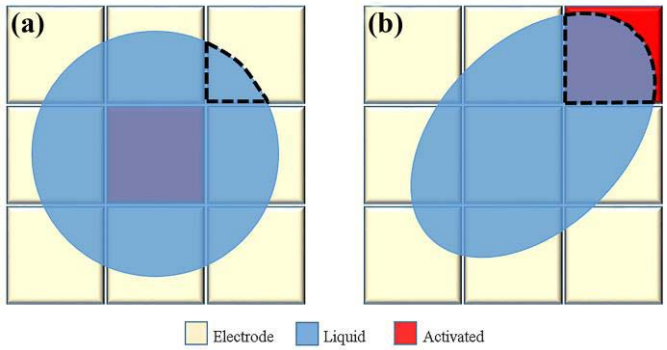

Fig. 3. Droplet shape on one tested electrode region when (a) V_{AC} was applied to the centered electrode; (b) V_H was applied to the non-centered electrode. The area enclosed by dotted lines represents the partial region where the liquid covers on the buried electrodes.

the area percent of a droplet occupying on the buried electrode. $x_{liq} = 100\%$ represents that a droplet fully covers the buried electrode, *e.g.* the centered electrode. As a droplet's shape is unsymmetrical in practical, if V_{AC} is applied to the centered electrode and non-centered electrodes one by one, varied x_{liq}'s detection signals would be obtained. Through disposing these signals, the sensitivity of one electrode region can be gotten.

The whole chip's consistency can be obtained by repeating this measurement method at other on-chip regions.

Transformation is the other indispensable step. Normally, the actuating voltage $V_{AC} = V_H$ is higher than V_{th}. When measuring the liquid's fractions on those non-centered electrodes under V_H, the liquid will distort and slide, which is shown as the enclosed area in Fig. 3(b). Thus, great error will be induced if directly applying V_H. The execution of measuring the real fraction of the liquid will be severely blocked.

A relationship between V_{out} and V_{AC} in [17] indicates how to break through this dilemma.

The total current i_{tot} through the device can be expressed as

$$i_{tot} = kx_{liq}V_{AC} + bV_{AC} \tag{3}$$

where k and b are both constants.

Therefore, the detection signal V_{out} is

$$V_{out} = i_{tot}R_d = kx_{liq}R_dV_{AC} + bR_dV_{AC} \tag{4}$$

Eqn. (4) tells that at the same detecting electrode, no matter V_{AC} is V_H or V_L, V_{out} can be kept unchanged by properly adjusting the value of R_d. Thus, the exact liquid fraction x_{liq} can be measured under V_L as no distorting or sliding of the droplet exists. When using V_H as the actuation voltage, identical V_{out} indicates the same x_{liq} if R_d is properly adjusted. This simple transformation is the key to solve the above dilemma.

In the setup process of the system, calibrating the relationship between x_{liq} and V_{out} under V_L is conducted first. Then, by adjusting R_d, the identical V_{out} under V_H can be achieved. In applications of the system, only V_H is necessary. With the adjusted R_d fixed in the system, faults and barriers detection on a 10×10 array under V_H can be completed in 1s. The system shows potential in expanding to larger-scale 2D EWOD DMFs.

III. Experimental Results and Discussions

Experiments of system calibration and data visualization were carried out.

A. System Calibration

Our system's sensitivity and consistency are characterized in Fig. 4. It should be noted that as the 10×10 electrode array are numbered from Row 0-9 and Column 0-9, the electrode "mn" denotes the site of Row m and Column n.

To verify the relationship between V_{out} and V_{AC}, a deionized water droplet was placed on a selected region, where the centered electrode is 100% overlapped. Droplet volume was guaranteed by on-chip droplet dispensing [22] or a pipette (in this work). A 0 to 200 V_{pp} AC signal with a frequency of 1 kHz was applied to the centered electrode and V_{out} was recorded.

To obtain the sensitivity, *i.e.* the relationship between V_{out} and x_{liq}, the "42" centered region was selected to test. As the dielectric layer of the EWOD chip is 2μm SU-8 (SU-8 2002, MicroChem), the normal actuating voltage V_{AC}'s amplitude is roughly 200 V_{pp}. According to Section **II.B**, an AC signal of 100 V_{pp}, *i.e.* V_L, with a frequency of 1 kHz was applied to the non-centered and centered electrodes one by one. Droplet area fractions were measured by manually outlining the droplet profile and computing the pixel area via AutoCAD® 2014. Although not precise enough, this method is conventional [17], since the errors do not affect the practical applications. After measuring the fractions of droplet on every electrode in the region and recording the corresponding V_{out}, the relationship of V_{out} across x_{liq} was plotted. It should be noted that due to the leakage currents of SSRs, the V_{out} is not zero even if V_{AC} is not applied to the detected electrode. For analysis convenience, 0% droplet size is used to describe such state.

To investigate the system's consistency, the same experiments as the above one in eight different regions of the DMF were carried out in sequence, which almost covered the whole chip. The detection at every region was repeated ten times.

Experimental results are shown in Fig. 4. The maximum deviation of V_{out} for 10 time detections at every electrode is 7.53% but most of them are below 5‰. Fig. 4(a) is the optical images of "42" centered region on the PCB-EWOD chip. Around the magnified "42" centered region are the eight non-centered electrodes' images. Fig. 4(b) exhibits the relationship between V_{out} and V_{AC}. Fig. 4(c) is the relationship between V_{out} and x_{liq} of the "42" centered region. Fig. 4(d) shows the eight different regions' detection results.

As shown in Fig. 4(b), our system is linear, which verifies the equation (4) perfectly. In addition, the worsened leakage currents do not affect the system's detection performance. There still remains enough room between the "100% overlapped" line and the "without droplet" line when $V_{AC} = V_H$.

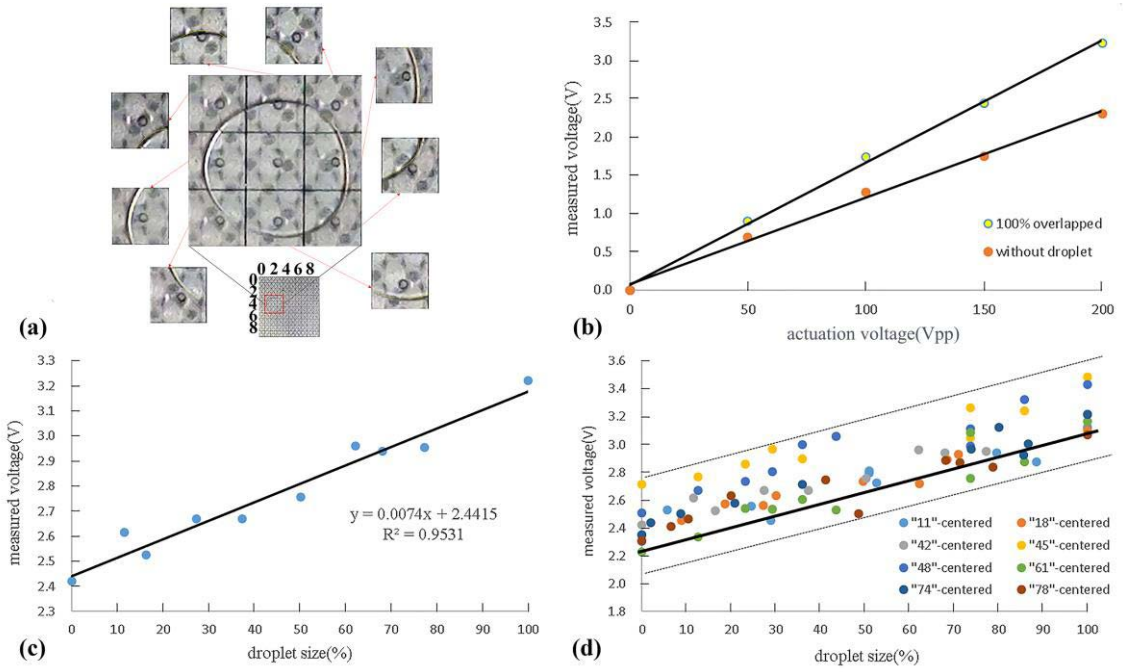

Fig. 4. Experimental results of detection sensitivity and consistency of the system. (a) Optical images of "42" centered region with eight non-centered electrodes on the PCB-EWOD chip; (b) V_{out} vs. V_{AC}. (c) Relationship between V_{out} and x_{liq}. (d) Detection results of eight different regions.

Good detection sensitivity and consistency on the whole chip can be observed in Fig. 4(c) and Fig. 4(d). The detection sensitivity of the "42"centered region was measured 7.4mV/%. Theoretically, our system that has 5mV resolution can distinguish 7‰ variation in droplet size, which is enough for quantitative analysis and detection of faults and barriers.

The measured V_{out} deviation among different electrodes on a same chip is inevitable as shown in Fig. 4(d). It is induced by the parasitic impedance of different geometries of connection paths and gap thickness discrepancy, *etc.* [17]. However, the effects of such deviations on the performance of the DMF can be eliminated by software auto-calibrating. This is due to that the expression of the sensitivity resulting from different regions can be compressed into one trend line. Here, as we set 40% droplets size and corresponding 2.5V as the cut-off value of x_{liq} and cut-off V_{out}, the standard line is $y = 0.0074x + 2.204$ (see the black solid line in Fig.4 (d)).

B. Sensing Faults and Barriers

The system's practical performances for sensing faults and barriers were explored. To eliminate the effects of the ADC limited input voltage and leakage currents on the detection results, we largely decreased R_d to widen measuring range of V_{out} in the later experiments.

On-chip dielectric breakdown faults and various barriers were all man-made. Liquid was dropped on the DMF surface randomly. The breakdown site was obtained through applying a sufficiently high amplitude AC signal to an electrode. Every detected electrode in the 10×10 array was measured nine times.

As shown in Fig. 5(a-i), the whole chip's detection results were normalized and plotted in 3D manner, while the insets are the corresponding optical images. It should be noted that all V_{out} are normalized by the V_{out} of site 99. Fig. 5(a) depicts a dry chip, while Fig. 5(b-d) are results of one, two and three small droplets, respectively. The breakdown site "63" is shown in the Fig. 5(e). When putting a droplet on it, some electrolytic bubbles appeared. Fig. 5(f-i) exhibits the results of one, two, four and seven big droplets, respectively. The maximum deviation of V_{out} for nine time detections at every electrode is 15.25%, while most of them are below 5%. It should be noted that the reason why deviation here increases nearly 10 times compared with Fig. 4 is that the greatly decreased R_d resulted V_{out} small in general.

Fig. 5(a) demonstrates that the detection results of the dry chip range from -3.09% to $+6.17‰$. We set up a cut-off value to present the faults and barriers, *i.e.* the measured results higher than 8.5% were painted in red.

According to equation (2), V_{out} is closely related to C_{di} and R_{di}. Once a barrier, *i.e.* a droplet, exists on a site, the site's C_{di} will increase simultaneously, which results in V_{out} growing up. As shown the red bars in Fig. 5(b-d, f-i), the site, of which V_{out} is higher than their surround sites', must own a barrier. The 8.5% cut-off value is based on the system calibration process. For dielectric breakdown site, *e.g.* Fig. 5(e), owing to largely decreased R_{di} and breakdown currents, all measured results on all electrode ($\sim$58) increase obviously compared to Fig. 5(f) ($\sim$51), although these two images have almost one same volume droplet on the electrodes.

The exact agreement between the regions occupied by the red bars and the distribution of various barriers and faults indicates our system can be further applied to larger-scale 2D EWOD DMFs.

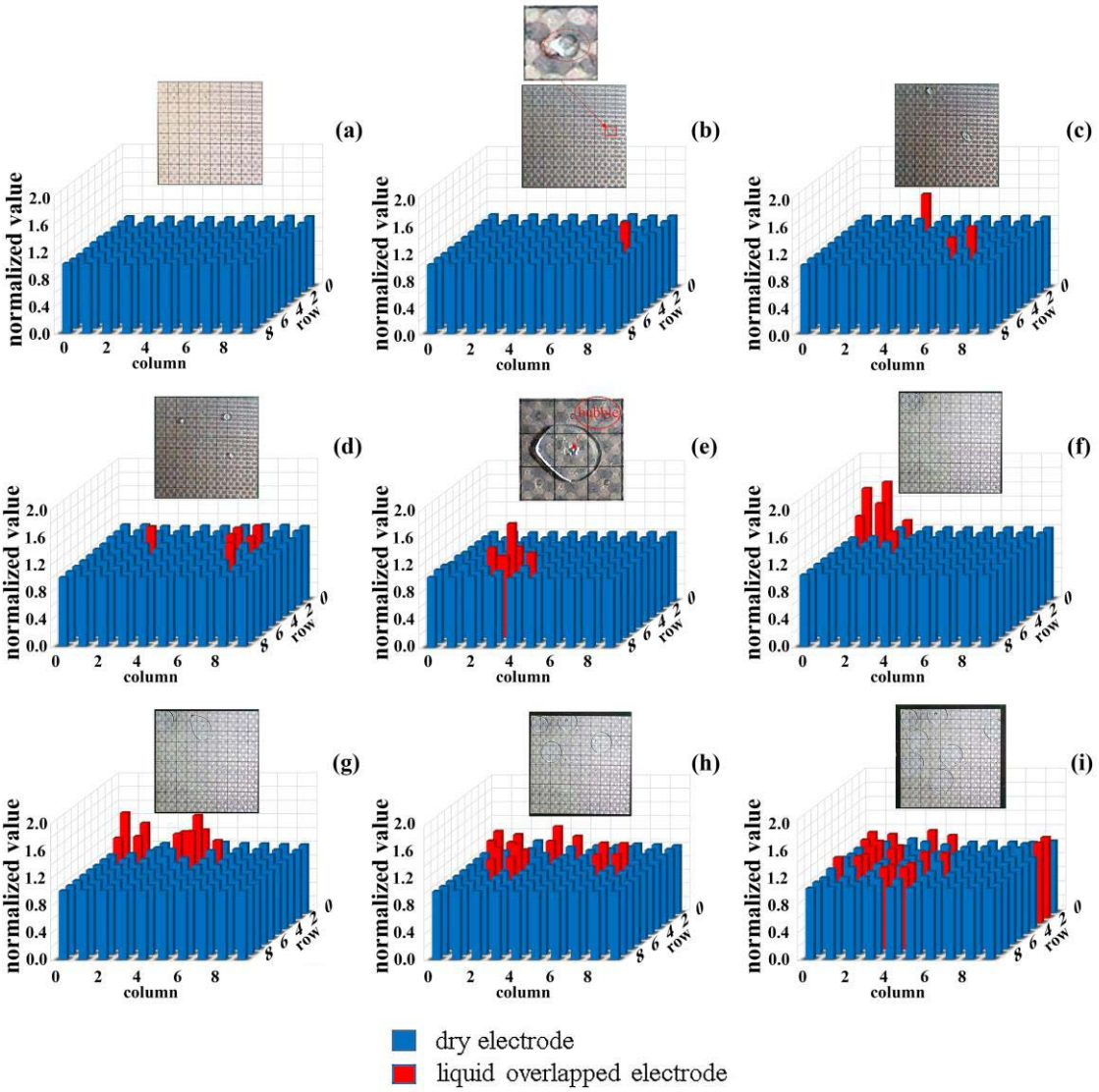

Fig. 5. Normalized results of all electrode sites for (a) dry chip; (b-d) chips with one, two and three small droplets; (e) breakdown site "63"; (f-i) chips with one, two, four and seven big droplets.

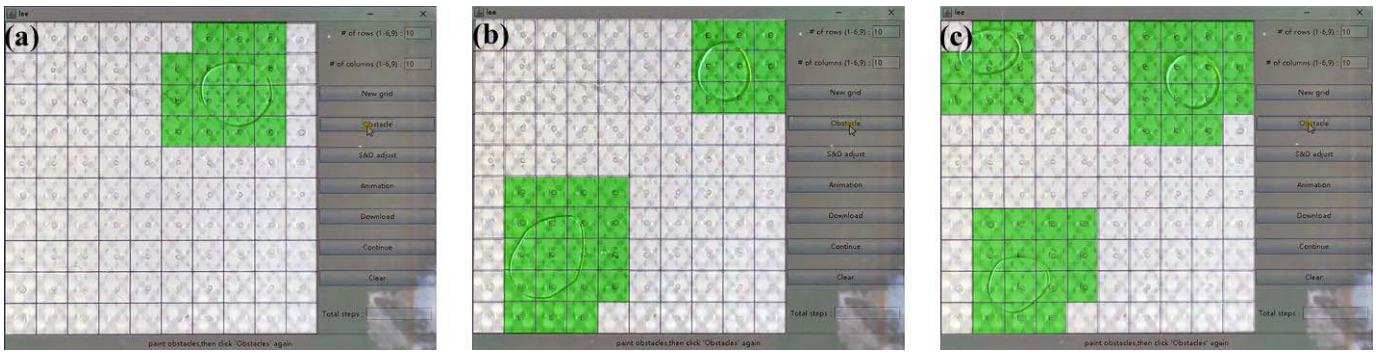

Fig. 6. Visualization of barriers with x_{liq} larger than 40% of electrode with (a)one droplet, (b) two droplets, and (c) three droplets.

C. Visualizing Faults and Barriers

Visualization of faults and barriers can be applied to auto-routing droplets on EWOD DMFs.

In the software, a cut-off V_{out} is set for defining the faults and barriers. The rule of electrode's neighbors that are forbidden to pass can also be decided in advance. Here is an example of visualization of the faults and barriers on the 10×10 DMF (see Fig. 6).

The actuation voltage V_{AC} was set to $220V_{pp}$ (V_H). 2.5V was set as the cut-off V_{out}. When the detection V_{out} is higher

than 2.5V, the electrode will be regarded as an "error" site, *i.e.* a fault or a barrier. Referring to the black solid line in Fig. 4(d), it represents a droplet covering more than 40% area of an electrode.

One, two and three barriers, *i.e.* droplets, were put on the PCB-EWOD chip in sequence. After launching the software, once clicking the "Obstacle" button, the detection results would be displayed on the interface in milliseconds. For comparison, we composited the PCB-EWOD chip's optical image with the software interface.

Fig. 6 is the pictures extracted from video S1 at 5s, 12s, and 21s, respectively. As expected, the number of displayed "error" sites is slightly greater than the real droplets occupied. This is due to the droplet movement constraints [2], which requires the "error" site's neighbors including non-diagonal adjacent electrodes and diagonal adjacent electrodes forbidden to interact. Further details about visualizing faults and barriers are provided in the video S1.

IV. Conclusions

In applications of EWOD DMFs, faults and barriers influence the experiment results directly. In this work, we analyzed the on-chip faults and barriers detection theory and presented a specific voltage transforming method. This novel method can be used in fast calibrating large-scale 2D EWOD DMFs.

We have successfully designed and implemented a low-cost and portable sensor-free system combining hardware and software for fault and barrier detection on the 10×10 DMF. 7.4mV/% droplet detection sensitivity was achieved and good consistency was observed. The detection results of various barriers and faults agree well with the real error distribution on the EWOD chip. Furthermore, a simple application of visualizing faults and barriers was carried out, which is helpful for developing automated EWOD DMFs.

Such system meets the needs of low price and large-scale of DMF for lab on chip, especially point-of-care applications. It shows great potential in developing the merging automated 2D EWOD DMFs.

References

[1] G. Wang, D. Teng, Y.-T. Lai, Y.-W. Lu, Y. Ho, and C.-Y. Lee, "Field-programmable lab-on-a-chip based on microelectrode dot array architecture," *IET Nanobiotechnol.*, vol. 8, no. 3, pp. 163–171, 2013.

[2] Y. Zhao and K. Chakrabarty, *Design and Testing of Digital Microfluidic Biochips*. New York, NY, USA: Springer, 2013, pp. 27–29.

[3] V. Shukla, N. B. B. Z. Ali, F. A. Hussin, N. H. Hamid, and M. A. Sheikh, "Fault modeling and simulation of MEDA based digital microfluidics biochips," in *Proc. 29th Int. Conf. VLSI Design 15th Int. Conf. Embedded Syst.*, Kolkata, India, Jan. 2016, pp. 469–474.

[4] P. S. Dittrich and A. Manz, "Lab-on-a-chip: Microfluidics in drug discovery," *Nature Rev. Drug Discovery*, vol. 5, no. 3, pp. 210–218, Mar. 2006.

[5] J. Gao *et al.*, "An intelligent digital microfluidic system with fuzzy-enhanced feedback for multi-droplet manipulation," *Lab Chip*, vol. 13, no. 3, pp. 443–451, 2013.

[6] K. Hu, B.-N. Hsu, A. Madison, K. Chakrabarty, and R. Fair, "Fault detection, real-time error recovery, and experimental demonstration for digital microfluidic biochips," in *Proc. Design, Autom. Test Europe Conf. Exhib. (DATE)*, Grenoble, France, Mar. 2013, pp. 559–564.

[7] K. Hu, M. I. L. Chen, Z. Li, K. Chakrabarty, and R. Fair, "Experimental demonstration of error recovery in an integrated cyberphysical digital-microfluidic platform," in *Proc. IEEE Biomed. Circuits Syst. Conf. (BioCAS)*, Atlanta, GA, USA, Oct. 2015, pp. 1–4.

[8] T. Xu and K. Chakrabarty, "Integrated droplet routing in the synthesis of microfluidic biochips," in *Proc. DAC*, 2007, pp. 948–953.

[9] O. Keszocze, R. Wille, T.-Y. Ho, and R. Drechsler, "Exact one-pass synthesis of digital microfluidic biochips," in *Proc. DAC*, 2014, pp. 1–6.

[10] D. Grissom and P. Brisk, "Fast online synthesis of generally programmable digital microfluidic biochips," in *Proc. CODES+ISSS*, 2012, pp. 413–422.

[11] K. Y.-T. Lai, Y.-T. Yang, and C.-Y. Lee, "An intelligent digital microfluidic processor for biomedical detection," *J. Signal Process. Syst.*, vol. 78, no. 1, pp. 85–93, 2015.

[12] Z. Li, K. Y.-T. Lai, P.-H. Yu, T.-Y. Ho, K. Chakrabarty, and C.-Y. Lee, "High-level synthesis for micro-electrode-dot-array digital microfluidic biochips," in *Proc. 53nd ACM/EDAC/IEEE Design Autom. Conf. (DAC)*, Austin, TX, USA, Jun. 2016, p. 146.

[13] Z. Li, K. Y.-T. Lai, P.-H. Yu, K. Chakrabarty, T.-Y. Ho, and C.-Y. Lee, "Droplet size-aware high-level synthesis for micro-electrode-dot-array digital microfluidic biochips," *IEEE Trans. Biomed. Circuits Syst.*, vol. 11, no. 3, pp. 612–626, Jun. 2017.

[14] B. Hadwen *et al.*, "Programmable large area digital microfluidic array with integrated droplet sensing for bioassays," *Lab Chip*, vol. 12, no. 18, pp. 3305–3313, 2012.

[15] S. Kalsi *et al.*, "Rapid and sensitive detection of antibiotic resistance on a programmable digital microfluidic platform," *Lab Chip*, vol. 15, no. 14, pp. 3065–3075, 2015.

[16] V. Shukla, F. A. Hussin, N. H. Hamid, and N. B. B. Z. Ali, "Investigation of capacitance dependence on droplet volume in MEDA based biochips," in *Proc. 6th Int. Conf. Intell. Adv. Syst. (ICIAS)*, Kuala Lumpur, Malaysia, Aug. 2016, pp. 1–5.

[17] S. Sadeghi *et al.*, "On chip droplet characterization: A practical, high-sensitivity measurement of droplet impedance in digital microfluidics," *Anal. Chem.*, vol. 84, no. 4, pp. 1915–1923, Jan. 2012.

[18] S. C. C. Shih, R. Fobel, P. Kumar, and A. R. Wheeler, "A feedback control system for high-fidelity digital microfluidics," *Lab Chip*, vol. 11, no. 3, pp. 535–540, 2011.

[19] R. Fobel, C. Fobel, and A. R. Wheeler, "DropBot: An open-source digital microfluidic control system with precise control of electrostatic driving force and instantaneous drop velocity measurement," *Appl. Phys. Lett.*, vol. 102, no. 19, pp. 193513-1–193513-4, 2013.

[20] H. Ren, R. B. Fair, and M. G. Pollack, "Automated on-chip droplet dispensing with volume control by electro-wetting actuation and capacitance metering," *Sens. Actuators B, Chem.*, vol. 98, no. 2, pp. 319–327, 2004.

[21] J. Gong, "All-electronic droplet generation on-chip with real-time feedback control for EWOD digital microfluidics," *Lab Chip*, vol. 8, no. 6, pp. 898–906, 2008.

[22] W. Wang, J. Chen, and J. Zhou, "An electrode design for droplet dispensing with accurate volume in electro-wetting-based microfluidics," *Appl. Phys. Lett.*, vol. 108, no. 24, pp. 243701-1–243701-5, 2016.

Chunqiao Li is currently pursuing the degree with the State Key Laboratory of ASIC and Systems, School of Microelectronics, Fudan University. His research interest focuses on biochemical application based on microfluidic technology, EDA (IC and digital microfluidic), and smart system.

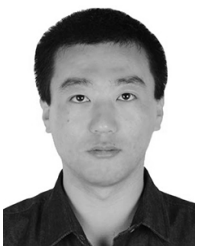

Wei Wang is currently pursuing the degree with the State Key Laboratory of ASIC and Systems, School of Microelectronics, Fudan University. His current research focus on the design, optimization, and integration with lab on a chip tools for diagnostics in EWOD microfluidics systems.

Lei Chao received the M.S. degree from the State Key Laboratory of ASIC and Systems, School of Microelectronics, Fudan University. She is currently with NXP Semiconductors. Her research interest focuses on novel biodegradable/biocompatible materials used in EWOD devices.

Xiumin Ji received the M.S. degree from the State Key Laboratory of ASIC and Systems, School of Microelectronics, Fudan University. She is currently with AMD. Her research interest focuses on novel dielectrophoresis devices.

Jia Zhou received the Ph.D. degree from Fudan University in 2004. She is currently a Full Professor with the School of Microelectronics, Fudan University. Her research interests are in the areas of MEMS/NEMS-based chemical, biochemical, and biomedical sensors and their applications, including EWOD digital microfluidics based systems, high frequency ultrasonic array transducers, piezoelectric microcantilvers, and electrochemical immunosensing systems.